Morphogenesis of the gastrovascular canal network in Aurelia jellyfish: Variability and possible mechanisms

Solène Song, Stanislaw Żukowski, Camille Gambini, Phillipe Dantan, Benjamin Mauroy, Stéphane Douady, Annemiek Johanna Maria Cornelissen

frontiers | Frontiers in Physics

TYPE Original Research
PUBLISHED 09 January 2023
DOI 10.3389/fphy.2022.966327

OPEN ACCESS

EDITED BY
Pau Formosa-Jordan,
Max Planck Institute for Plant Breeding Research, Germany

REVIEWED BY
Florian Goirand,
Technical University of Munich, Germany
Raghunath Chelakkot,
Indian Institute of Technology Bombay, India
Luis Diambra,
National University of La Plata, Argentina

*CORRESPONDENCE
Annemiek J. M. Cornelissen,
annemiek.cornelissen@u-paris.fr

SPECIALTY SECTION
This article was submitted to Biophysics, a section of the journal Frontiers in Physics

RECEIVED 10 June 2022
ACCEPTED 30 November 2022
PUBLISHED 09 January 2023

CITATION
Song S, Żukowski S, Gambini C, Dantan P, Mauroy B, Douady S and Cornelissen AJ (2023), Morphogenesis of the gastrovascular canal network in *Aurelia* jellyfish: Variability and possible mechanisms.
Front. Phys. 10:966327.
doi: 10.3389/fphy.2022.966327

Morphogenesis of the gastrovascular canal network in *Aurelia* jellyfish: Variability and possible mechanisms

Solène Song[1], Stanisław Żukowski[1,2], Camille Gambini[1], Philippe Dantan[1], Benjamin Mauroy[3], Stéphane Douady[1] and Annemiek J. M. Cornelissen[1]*

[1]Laboratoire MSC, UMR 7057, Université Paris Cité—CNRS, Paris, France, [2]Faculty of Physics, Institute of Theoretical Physics, University of Warsaw, Warsaw, Poland, [3]Laboratoire J. A. Dieudonné, UMR 7351, Université Côte d'Azur—CNRS, Vader Center, Nice, France

Patterns in biology can be considered as predetermined or arising from a self-organizing instability. Variability in the pattern can, thus, be interpreted as a trace of instability, growing out from noise. Studying this variability can, thus, hint toward an underlying morphogenetic mechanism. Here, we present the variability of the gastrovascular system of the jellyfish *Aurelia*. In this variability emerges a typical biased reconnection between canals and time-correlated reconnections. Both phenomena can be interpreted as traces of mechanistic effects, the swimming contractions on the tissue surrounding the gastrovascular canals, and the mean fluid pressure inside them. This reveals the gastrovascular network as a model system to study the morphogenesis of circulation networks and the morphogenetic mechanisms at play.

KEYWORDS

morphogenesis, gastrovascular, network, jellyfish, instabilities, variability, mechanical constraints

1 Introduction

Morphogenesis remains an important question in biology. Independently of how the phenotype can be selected through natural selection, it remains essential to understand how it can appear, develop from its original fertilized egg, and get its own shape. Since humans observe nature, they classify similar shapes into species. Within one species, the shape is robustly perpetuated across generations. So, biological shapes are constrained enough within one species. Even with the discovery of many genes and produced molecules and their important role in morphogenesis, how these constraints are applied to guarantee a given result is not completely clarified. In particular, how a complex shape can appear while being constrained remains obscure [1]. A complex shape would need much information to be described, thus many regulations to achieve it. However, the unfolding in time of instability can lead to a regulated complex shape from a simple mechanism [2].

In his pioneering work, Alan Turing proposed that even if some morphogenesis can be implemented through the various concentrations of some chemical products, the pattern they present is created by a spatial instability [3]. This means that even if the original distribution of chemicals is homogeneous, this state will be unstable and spontaneously goes into patches of different concentrations. Also, the pattern is spontaneously created, not controlled: only its global characteristics, such as wavelength, which depends on the reactions and diffusion characteristics of the chemicals are set, not its particular position.

This view may seem contradictory with the constrained production of a stereotyped shape. However, many examples of fluctuating shapes can give the intuition of an underlying instability. In this study, this is the case we present for the formation of the gastrovascular network of the jellyfish *Aurelia*. Jellyfishes are very old life-forms that appeared before the "vertebrate" revolution but already present a complex vascular structure. This vascular structure is an open circuit, perfusing the whole body from the open mouth to the stomach pouches and back [4, 5]. The flow in this circuit is due both to the effect of the whole contraction of the body and to the action of many cilia on the internal epithelium. These canals, in a body plan which is basal in the animal tree, can be seen as an early simple model of a network of tubes with a transport function as the later evolved closed vascular networks such as the blood vascular network.

This gastrovascular canal network develops while the jellyfish grows from its first ephyra stage. This ephyra stage emerges from a sessile polyp [5, 6]. During the transformation of the polyp into jellyfish (a process called strobilation), this polyp is subjected to instability that creates many disks along its axial body, each disk being unstable in the radial direction and forming arms (lobes with two marginal lappets), of typical 8-fold symmetry. One after the other, the top disk further transforms and detaches, resulting in a free swimming jellyfish larva, the ephyra. This way of generation ensures that a series of jellyfish appears from a very same polyp, so they are clones. The development of the gastrovascular canal can be followed while the jellyfish goes from a star-like shape ephyra of a few mm diameters to a juvenile jellyfish of approximately 10 mm, which has just reached the circular shape of adult medusa to a mature jellyfish of about 100 mm.

We will focus on the growth of the pattern from juvenile, with few rather stereotyped canals, to adult, with many canals. The formation of the network before the juvenile stage has complex but more regular steps [5] and is not considered in this study. Subsequent growth happens with the sprouting of new canals and their reconnection with the rest of the system. There is a strong tendency for a sprouting canal to reconnect to the younger neighbor, leading in an ideal case to a particular fractal pattern. However, this bias is not absolute, and there are many variations. With the observation of these dynamics and their results of complex and varying shapes, we can get closer to the origin of the morphogenetic process. More precisely, the question of which phenomena can be responsible for the development of these shapes can be studied. In the following, we will present two possible phenomena with both some interests and limitations.

2 Canal network morphogenesis

2.1 Stereotypical morphology

The gastrovascular canal network in juvenile jellyfish can be presented with a stereotypical structure (see Figure 1A). In 1/8th of the jellyfish (an octant), there is radially one gastric pouch of the stomach (or the junction between two pouches) near the center, and a marginal ring canal, circling around the whole rim of the jellyfish. Radially, there are two canals, rather straight and unbranched, joining the side of the pouches to the marginal ring canal, the adradial canals. Between such two straight canals, there is a canal joining the gastric pouch (interradial canal) or directly in the mouth opening at the pouch junction (perradial canal) to the marginal ring canal and a rhopalium (a sensory organ that can be caricatured as an "eye"). These canals present, in the juvenile stage, two secondary side branches connecting the main inter or perradial canal with the ring canal, forming a trifurcation. There is no apparent difference between interradial and perradial morphologies. We will, thus, simply call them "trifurcate" canals (in contrast we can call the adradial canals the "straight" canals). In juveniles, new canals mainly sprout from the marginal ring canal and connect to one of the surrounding already existing radial canals.

After growth, for adult jellyfishes, it is tempting to present its shape as a regular, fractal one. Although a perfect one is rare, it can be sometimes observed in small jellyfish (we found occurrences in nature or in the Cherbourg Aquarium culture). The best way to understand it is, as for fractals, to describe its construction, step by step, with canals connecting to each other in a well-defined and precise order (Figure 1B). In the juvenile stage (Figure 1A) at the ring canal, the trifurcation cut the interval between the two straight canals in four. Roughly four new canals sprout from the ring canal, grow in these intervals, and connect either left or right to the two younger side canals of the fork. The next generation of eight canals would also connect to the last previous generation, leading to a distinctive tree shape (Figure 1B).

There is a strong tendency, around 80% of the cases (Figure 1C and Supplementary Material), for the new sprouting canals to connect to the younger radial canal at proximity. If we look at the distribution of "false" connections, that is, canals not connecting to the younger canal at proximity, per octant, we find the very asymmetric

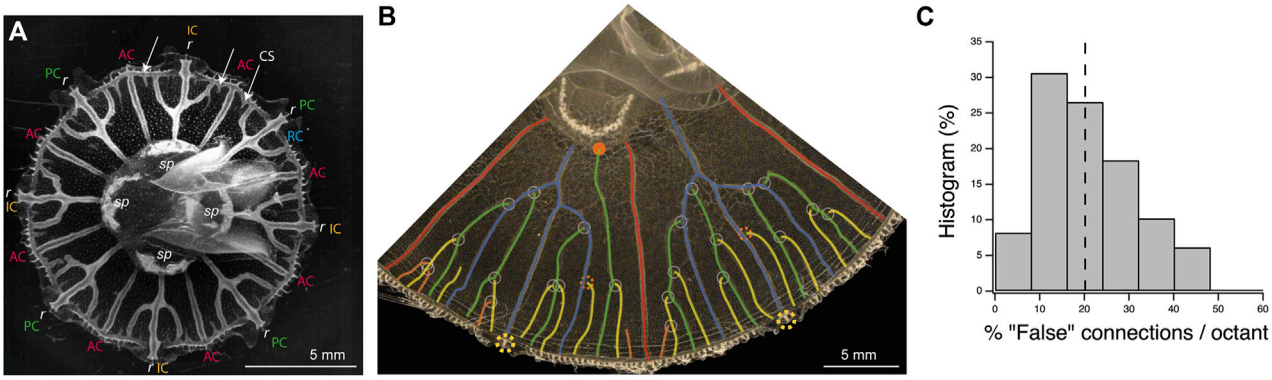

FIGURE 1
Structure and morphogenesis of the canal network of the gastrovascular system of the jellyfish *Aurelia*. **(A)** Picture of a juvenile jellyfish showing the structure of the gastrovascular system. There are typically four stomach pouches (*sp*), eight sensory organs, or rhopalium (*r*). At the periphery of the jellyfish there is a ring canal (RC in blue). Connecting this ring canal, from the sides of the stomach pouches, there are typically eight straight adradial canals (AC in red). Between these adradial canals, other canals connect either the stomach pouch, the perradial canal (PC in green), or the junction between two stomach pouches, the interradial canal (IC in orange), to the rhopalia. New canal sprouts (CS) sprout from the ring canal (arrows). **(B)** Picture of two octants of a later developmental stage (original in Supplementary Figure S2). The sprouting canals have reconnected to older ones, forming branched perradial and interradial canal systems (rhopalia, yellow dashed circles; adradial canals, and red; original trifurcate canals, blue). The sprouting canals have the tendency to reconnect to the youngest side canal (white circles), leading in theory to a specific fractal tree shape. The four (green) canals sprouting in the two intervals between the fork and the two intervals near the side straight canals (red) would connect to side branches of the original (blue) fork. The next eight canals (yellow) would connect to the previous one (green). Also, the next generation (orange) would connect to the previous one (yellow). Some connections do not follow this pattern and either reconnect to older ones (dashed red circles) or even directly to the stomach pouch (red disk). Some irregular growth is also visible on the left (perradial canals), leading to mixing of generations, as some fourth (orange) canals have already appeared, and even connected, while some third order (yellow) generations have not appeared yet or reconnected. **(C)** Histogram of the percentage of "false" connections (i.e., canal connections not made to the closest younger canal) in midsize jellyfish as in B, per octant (seven jellyfish with eight octants and one with nine octants $n = 65$ octants). There are, for instance, 10% of octants present between 32% and 40% of false connections. The median value (dashed line) is 20%.

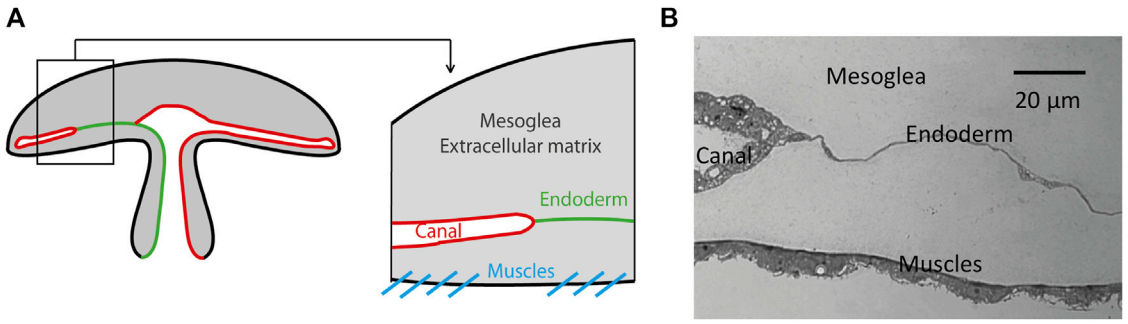

FIGURE 2
Anatomical position of the canals in the jellyfish *Aurelia*. The canals are surrounded by an endodermal layer positioned just above the lower *epidermis* with muscles. **(A)** Schematic representation. **(B)** Optical view of a histological 4 µm thick microtome slice of a fixed jellyfish.

distribution of Figure 1C. This indicates that it is a real bias and that the false connections accumulate independently, making it more probable to have only few false connections (but rare to have none) and rarer to have more false connections. The essential question arising from this structure and its development is to understand why new canals would connect to the younger previous ones.

2.2 Differential contraction

To understand this differential connection of the sprouting canal to the youngest close one, a first observation on the morphology and appearance of the canal itself is helpful. The canals, consisting of a canal wall with a monolayer of dense canal cells around a lumen, are situated inside a monolayer cell

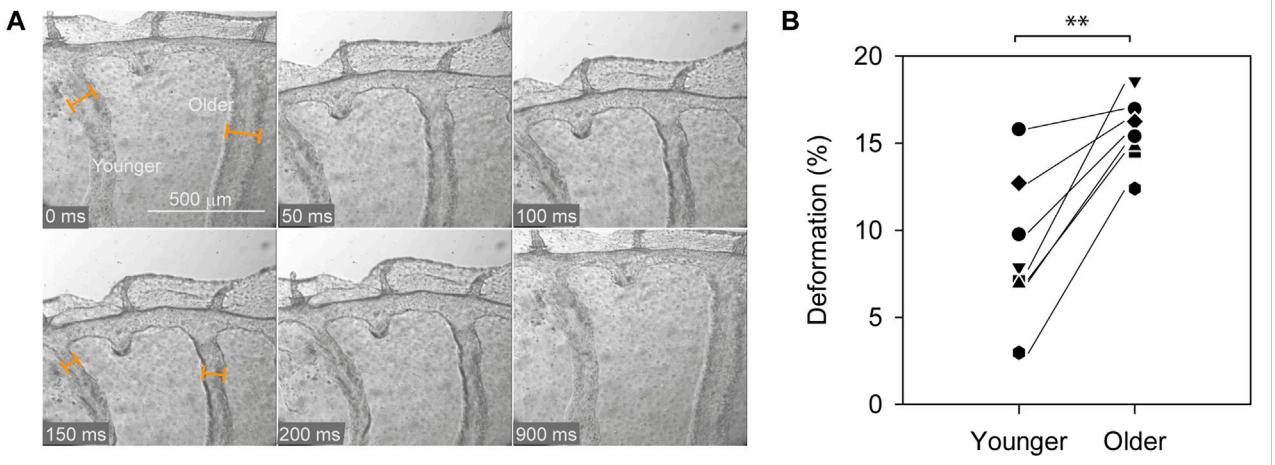

FIGURE 3
Relative contraction of canals during jellyfish swimming contraction. **(A)** A sequence of pictures showing a young and an older canal pictured during a contraction (with also a canal sprout in between). Canal width measurement during the resting phase and the maximum contraction allows measuring the relative contraction of the canals. **(B)** The pairwise measurement shows that the contraction of a young canal is significantly smaller than the one for older canals ($p < 0.01$, one-way repeated measures Anova, followed by a Student–Newman–Keuls test for a pairwise multiple comparison).

sheet with largely spread endodermal cells (see Figure 2). We have observed that the canal sprouts are growing in the endodermal sheet with cell proliferation around the tip of the canal [7].

The second important point for a possible morphogenetic mechanism is that these canals are growing while the jellyfish is growing, and it is growing while being, since the beginning, actively contracting, to swim and gather food. These contractions from a nearly flat state to a bell shape are done by a muscle sheet contracting and reducing the periphery perimeter. These movements then induce a considerable mechanical deformation to the endodermal layer, containing the canals, which is just above this muscle layer (Figure 2).

A proposed mechanism for the bias in connections is that the mechanical response to the contraction during swimming is different for different parts of the tissues. We propose that the endodermal cells which are not part of canals are submitted to a high mechanical stress as they are nearly incompressible, being held by the incompressible, but soft, upper and lower mesoglea [8]. On the contrary, canals are not flat; they enclose a lumen which protrudes out from the endodermal sheet (Figure 2B). Measurements during contractions show that the older the canal, the more deformable it is (Figures 3A,B). We propose this property as the cause of the bias leading growing canals to connect more frequently to younger canals than to older ones.

2.3 Simulating contraction

To see the effect of the differential contractibility of the canals, we analyzed the distribution of the stress in the jellyfish during muscle contractions. To do so, we build a mechanical model of the endoderm and of the canals of the jellyfish. The effects of the mesoglea elasticity and muscle contractions are injected through the boundary conditions.

The model geometry is limited to a slice of the endoderm near the ring canal. The endoderm slice is represented by a ring at the edge of a circular disk (Figure 4A), extending 1/5 of the jellyfish radius. We neglect the local convexity of the endoderm, approximating it with a plane surface. During swimming, the umbrella reduces its radius, increasing the convexity, but we assume it remains flat. The geometry of the canals and sprout were chosen to be coherent with our observations in a juvenile jellyfish of 1 cm diameter (see Supplementary Figure S7A).

The model follows the law of mechanics: $\rho \frac{\partial^2 u}{\partial t^2} - div(\sigma(\epsilon)) = 0$, where ρ is the density of the endoderm (assumed to be similar to that of water), u is the displacement of the material, $\varepsilon = \nabla u$ is the relative displacements of the material (strain), and $\sigma(\varepsilon)$ is its stress–strain relationship. To close the model, we further use the Hooke's law of elasticity to express the stress as a function of the strain. Since we are not interested in the global bell shape of the jellyfish and its change during the muscle contractions and spring back mediated by the mesoglea elasticity [8], we neglect the stress components in the direction normal to the (flat) endoderm surface, that is, $\sigma_z = 0$, $\sigma_{xz} = 0$, and $\sigma_{yz} = 0$. As a consequence, our model is a 2D model and Hooke's law reduces to

$$\sigma_x = \frac{E}{1-\nu^2}\left(\epsilon_{xx} + \nu\epsilon_{yy}\right),$$
$$\sigma_y = \frac{E}{1-\nu^2}\left(\epsilon_{yy} + \nu\epsilon_{xx}\right),$$

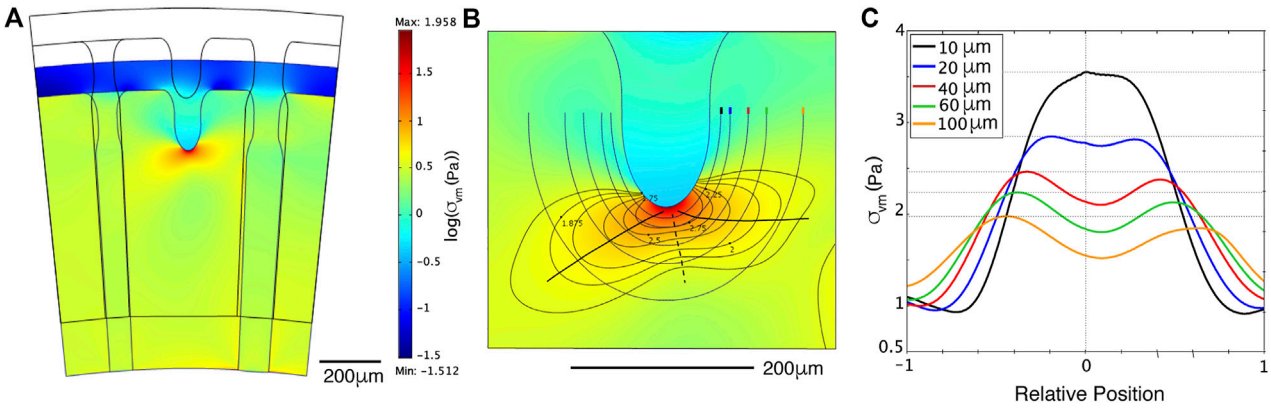

FIGURE 4
Stress distribution predicted by numerical simulations **(A)**: Finite element simulation with stiffer young canal (left) and softer old canal (right). The contraction is reproduced by reducing the radial distance with a constant angle, thus reducing the orthoradial one. The log of the mechanical stress (colored scale) is smaller (blue-green) in the soft right canal, and reduced around the sprouting canal (light blue), but concentrated at its tip (red spot). **(B)**: A zoom of the stress around the tip. Level lines, circling away the red spot reveal two lobes, one forward left to the young canal, one right to the old canal. Lines drawn at fixed distances are drawn with each its color code, to measure the stress along them. The two stress maximums and minimum along these successive lines are indicated by black full and dotted lines, respectively. **(C)**: The stress measured along these lines, centered on the axial position of the tip and rescaled from beginning to end, with their colors, and the distance to the finger indicated. Horizontal dotted lines show that the left maximum toward the young canal is always higher. This will turn the propagation of the new canal sprout toward the younger, stiffer one.

$$\sigma_z = 0,$$
$$\sigma_{xy} = \frac{E}{1+\nu}\epsilon_{xy},$$
$$\sigma_{xz} = 0,$$
$$\sigma_{xz} = 0,$$

with E being Young's modulus and ν Poisson's ratio. The observed difference of deformability (Figure 3) was translated into plausible elastic Young's moduli and Poisson ratio. We assume the endoderm as a flat rigid nearly incompressible elastic sheet. The near incompressibility in the plane is given by Poisson's ratio $\nu_{en} = 0.49$ and the rigidity by Young's modulus $E_{en} = 100\ Pa$. We modeled the canals in 2D by a compressible elastic membrane, with a lower Young's moduli than the endoderm. The chosen Poisson's ratio of the canals of 0.3 ($\nu_{yc} = \nu_{oc} = 0.3$; ν_{yc} being the Poisson's ratio for the young canal and ν_{oc} the Poisson's ratio for the old canal), allows for compression in the plane, translating the vertical expansion of the canals. The Young's modulus of the young canal is assumed to be stiffer with $E_{yc} = 30\ Pa$ than the old canal, for which $E_{oc} = 10\ Pa$.

The muscular orthoradial contraction is mimicked *via* the boundary conditions as shown in the Supplementary Figure S7B. To simplify, instead of compressing the whole two radial borders of the slice, we only reduce the radial position of the outer circular boundary. Following our observations, we typically reduce it by 200 µm in one second. The sides of the ring slice can only slip along the radial axis, and the inner circular boundary is free to move ($\sigma(\epsilon).n = 0$, with n the outer normal of the boundary). As a result, the whole slice compresses after one second. At the end of the contraction, the circular deformation is 4% at the outer edge (top of ring canal) and 5% at the inner edge. With these characteristics, the simulation can be performed quasi-statically. The model of contraction was studied with a numerical simulation based on finite elements.

The results show an accumulation of stress at the tip of a new canal (the stress is partly released at the sprouting canal, and all the residual stress around focuses on the tip), and the stress is slightly different in the two surrounding canals of different age/stiffness (Figure 4A). At the tip, the stress shows two lobes, toward both side canals, the one toward the younger canal being larger and more intense (Figure 4B). The quantitative result is that the maximum of stress is shifting toward the younger stiffer canal (Figure 4C). Based on these observations, we propose that high stress will guide the canal sprout to grow toward the younger stiffer radial side canal.

3 Variability

Since the connection of the sprouting canal to a younger close one is only a strong bias, there are many variations of patterns and only rarely a perfect one. Looking more generally at *Aurelia* jellyfish from different origins and growth conditions (see Section 6) also reveals variable patterns. The observed patterns display more variability than what we would expect from the previously described process based on successive sprouting of new canals from the rim and connection to the youngest neighboring canal.

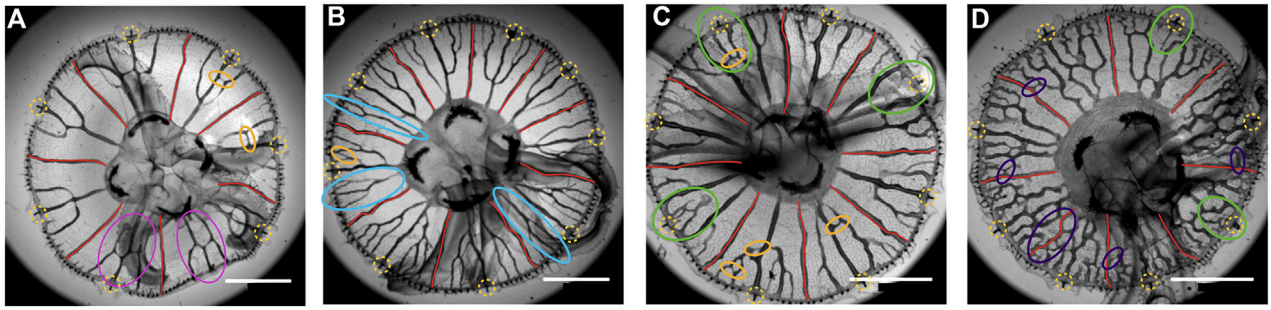

FIGURE 5
Four *Aurelia* specimens of around the same size, from Cherbourg. The rhopalia are surrounded by yellow-dashed circles, and the adradial canals are drawn in red. In **A**, the continuation of canals after connecting to the central one is indicated by pink ellipses. In **(A–C),** some interconnection between canals, forming loops, is indicated (orange ellipses). In **B**, some side canals never reconnect to the central one and connect directly to the stomach pouch (light blue ellipses). In **(C**,**D)**, some rhopalia are not connected to canals (green ellipses). In **D**, there are many meandering canals and reconnections making many loops, in particular reconnections with straight adradial canals (violet ellipses). Scale bar 5 mm.

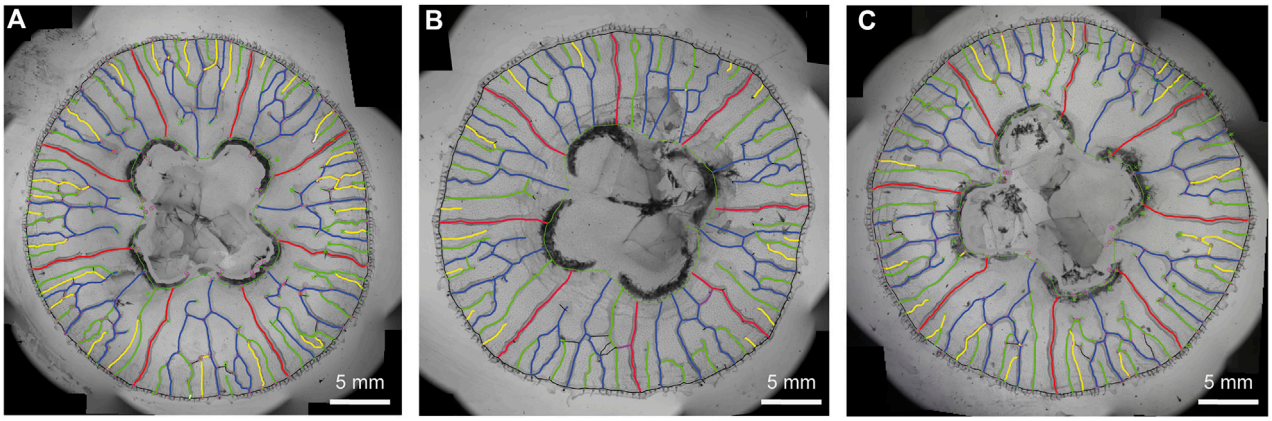

FIGURE 6
Three clones from the same polyp. **(A–C)** The pattern has been interpreted for easier comparison. As in Figure 1B, the adradial canals are drawn in red; the central canal, and the first side canals forming the trifurcation are drawn in blue; the second generation in green; the third in yellow. One can observe many irregularities as in Figure 5: side canals not reconnecting to the central one, reaching (or going to reach) the stomach pouch, interconnections to straight canals [violet, in **(B)**] and to other radial canals (black) making loops. All these irregularities, although similar in the three clones, are in detail different.

Figure 5 shows four cases giving an indication of the large variety of patterns. As a source of variability, one can observe that, even after reconnecting, the side canals would keep growing toward the stomach (pink ovals in Figure 5A). Another variation is the presence of meandering canals that are potential sites for the growth of new canals. Both modes of growth induce the formation of loops on large (old) jellyfish, transforming the gastrovascular network into a foam-like pattern (Figure 5D). This creates patterns much more difficult to analyze.

An interesting point is that since there is a variability in these patterns, one can study where these variations originate from. In the case of ephyrae coming from a single polyp, which means they are clones and grown together, thus in identical conditions, one can look at resulting patterns. Here, we present three such clones grown together (Figure 6). One can observe a similar type of pattern but still differences. This shows that, even for genetically identical jellyfish and an identical environment, there is no strict control of the pattern. This suggests a self-organized pattern formation, relying on instability, amplifying the noise.

4 Canal breakthrough

A particular type of deviation from the stereotypical development is interesting to see dynamically. During development, one can observe that some canal sprouts do not

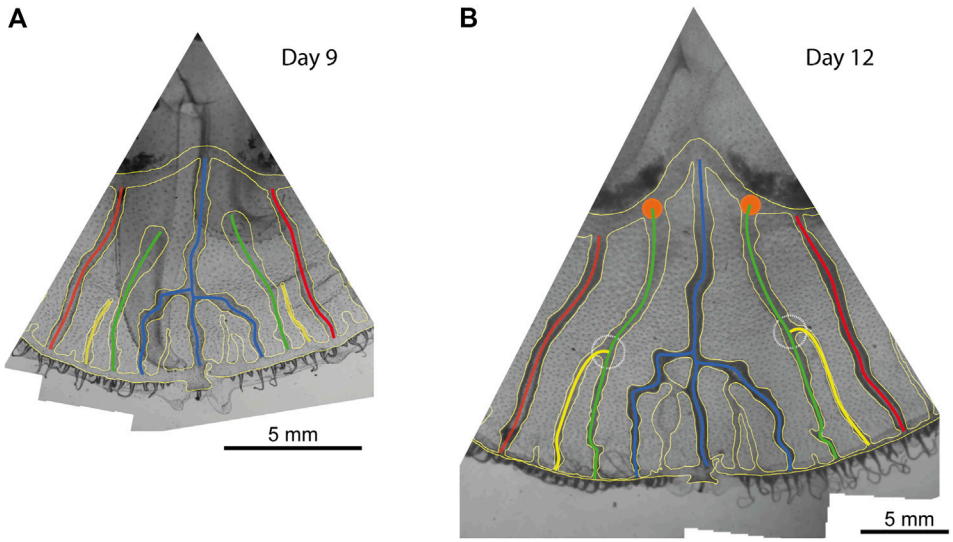

FIGURE 7
Two successive images of a jellyfish octant. **(A)** At day 9 of observation, secondary (green) side canals did not connect to the central ones and are reaching toward the stomach pouches. Similarly, there are two younger (yellow) canals growing aside of them without connecting either. **(B)** 3 days after, the side canals have reached the stomach pouch and connected (orange disks), and in the same period, the younger canals have also connected to these side canals (dashed white circles).

reconnect with the more central canals. Instead, they grow straight toward the stomach, independently from the other canals. It happens for the first-generation canals that sprout between the fork and the side adradial canals (see Figure 1B, Figure 5B), around 17% of the time (see Supplementary Material). Interestingly, in such a case, the next generation of side canals keeps growing independently too as long as the longest canal sprout did not reach the stomach pouch (see Figure 7A). However, as soon as the longest canal sprout reaches the stomach, it is observed that the smaller sprouts connect to the long canal that just got connected to the stomach (Figure 7B).

5 Discussion

When a pattern is constant, it is difficult to describe its origin and what controls it. On the contrary, variability helps get closer to the mechanisms producing these patterns. Here, we see that the pattern can be very variable, even in clonal jellyfish. That points to instabilities being at the origin of the pattern. Since Turing, we understand that instabilities mean that a homogeneous state is unstable, so that tiny inhomogeneities will grow to create a pattern. In this sense, instability starts with the amplification of noise. This first step results in a noisy pattern, which is a source of variability.

The further growth of the instability is often regulated by long-range interactions and global constraints (such as gradient of pressure). This leads to the growth of a regular pattern with a fixed wavelength for instance. This is how regular and reproducible patterns can appear, even if originating from an initial noise. In practice, this noise origin is often overlooked, and only regular patterns are studied theoretically. The most unstable regular pattern will be searched for, as it is the one most growing. Then, after a further restabilization, it will be the one finally observed. However, in some cases, the system keeps growing and being unstable, with no means of reorganization. This happens in physical systems, as in the Saffman–Taylor instability in circular geometry [9] or in biological growth, as in the lungs [10]. In such cases, the noise keeps being amplified, and variability can persist. This seems to be the case with the gastrovascular network of jellyfish.

There is still some regularity: the gastrovascular network can, under some growth conditions, follow a typical asymmetry (bias) and sometimes converge toward a stereotypical pattern. This comes from the interactions between canals, allowing regularization. However, we could guess that not following the bias comes from the presence of more noise, for instance, on the distance between canals, canal growth, and canal stiffness or resistivity. Such noise is well visible on Figure 1B, left, where successive generations of canals appear irregularly. This noise could blur the asymmetry and sometimes allows the sprouting canal to follow the second stress lobe (Figure 4), leading to a non-stereotypical connection. The fact that noise is the origin of these connections escaping the bias can be seen in the asymmetry of the distribution of Figure 1C. Noise leads to independent

misconnections, resulting into stereotypical octants with few mistakes but rarer octants with more numerous ones.

The sprouting of new canals from the circular ring canal also reveals instability of this ring that would be similar to the curving in the meandering canals, leading to local sprouting and later to other reconnections, forming small loops shunting the canals.

The fact that canals reconnect to each other is a particularly interesting phenomenon. The gastrovascular network is a tree structure connected to a ring canal. One would first imagine that it forms as a tree expanding with successive dichotomies of tips or side branching, and finally connecting to the ring canal. Here, we see a reverse growth: the branches appear from the ring canal, separated from each other, and reconnect only later. The reconnection between the canals leads to the formation of loops. The sprouting from other canals than the ring canal that further connect forms even more loops. This is interesting since the usual branching formation of trees, as in Laplacian growth [2], often forbids reconnection, hence the formation of loops [11]. Such reconnection is thus a particular phenomenon that deserves exploration.

This formation of loops by the reconnection of branches has to be differentiated from the case of stabilization and coarsening of loops. As for vascular remodeling from a capillary plexus [12], these systems start from homogeneously connected foam and particular dynamical evolution leads to the stabilization of large hierarchical loops [13–15]. Here, for the formation of loops by reconnection, the first mechanism proposed relates to cracks, which are known to reconnect [16], being related to two-dimensional stress [17], and leading to 2D-reticulated patterns [18, 19]. In this way, canals can be seen as the propagation of cracks in the endoderm. Stress accumulates at the tip of a new crack, and it is guided by the stress around it [16]. Here, too high stress at the tip of a sprout could induce the proliferation of cells [20, 21] and/or their transformation in canals cells, open the canals, and release the stress. The global stress field guides the movement of the tip of a new canal/crack. This relation to stress also explains the observed bias, that the crack is attracted to the larger stress, thus to the still stiff younger canal.

The second mechanism, even if related to Saffman–Taylor and Laplacian growth, would happen in the special case of resistive fingers [22]. This resistance creates gradients of pressure within the fingers. It allows connection of side fingers to a longer one when its pressure is locally lower. This particularly happens when the pressure in the longer one globally drops because of a connection to an outlet (breakthrough). This could explain the coincidence of a canal breaking through the stomach pouch and the reconnection of a side canal to it.

For the jellyfish canals, this would happen with the liquid pressure inside the growing canal sprouts during the muscle contractions in the orthoradial direction. However, when one canal sprout, in analogy with the Saffman–Taylor finger, reconnects directly to the stomach, then this transient high pressure at its tip drops to reach the pressure at the outlet, the stomach pouch. This dropping of pressure happens all along the canal, so that the lateral canal sprout can now perceive a place on the side with low pressure and be attracted to it.

These two mechanisms could be happening in the jellyfish or just be mechanical analogies of other phenomena. However, even from a mechanical point of view, they are not incompatible, being driven by the stress in the endodermal layer and the pressure in the canals, which are complementary parts of the mechanics of the network.

The source of large variability of the patterns, as shown in Figure 5, should also be investigated. Is it due to different growth conditions, growth histories, or also to different strains, revealing a different sensibility to mechanical constraints for instance?

Globally, these first observations show that the gastrovascular network results from a spontaneous organization, or, in other words, that it appears from instabilities, enhancing noise, so that two growths never produce the same result even with settings as close as possible (clones from a single polyp grown together in the same conditions). We consider that blood vascular networks in vertebrates [23–25] and venation in plant leaves [17] could result from similar spontaneous organization, however, with different detailed processes. Here, we show that there are clues that the morphogenesis of the gastrovascular pattern in the jellyfish could be related to mechanical processes, since it grows while the jellyfish is swimming with repetitive contractions. These contractions have clearly a mechanical effect on the tissue either by direct contraction or by a secondary effect on the flow inside the already existing canals.

6 Materials and methods

6.1 Jellyfish culture

Jellyfish *Aurelia aurita* were reared in the laboratory, at room temperature, in artificial seawater, produced by diluting 35 g or 28 g of synthetic sea salt (Instant Ocean; Spectrum Brands, Madison, WI) per liter of osmosis water (osmolarity 1,100 mOsm). Polyps of the Roscoff strain [26] were obtained by courtesy of Konstantin Khalturin from the Marine Genomics Unit, Okinawa Institute of Science and Technology Graduate University, Onna, Okinawa, Japan. Strobilation in polyps was induced by a lowering the temperature down to 10°C [27]. The newborn ephyrae were bred to adult stage. The measurements were performed on jellyfish at different sizes of juvenile jellyfish. Juvenile jellyfish had just reached the circular shape of adult medusas with a diameter of ~1 cm. Juveniles grow out into adult jellyfishes with fully developed stomach pouches.

Juvenile jellyfish (~1 cm in diameter) were obtained from the "Jellyfish Concept" in Cherbourg from their culture. The original polyps are extracted from the North Sea around Cherbourg. Juvenile jellyfish were bred to adults while growing. In the manuscript, we refer to these jellyfish as 'Cherbourg jellyfish'

when they originate from the Roscoff strain, we do not specify it in the manuscript.

6.2 Imaging of the gastrovascular canal network

The gastrovascular network of the jellyfish was observed using a Leica macro zoom (MACROFLUO LEICA Z16 APO S/No: 5763648) and a Photron Fastcam SA3 camera or directly using a Nikon D3300 camera with macro lens AF-S DX Micro NIKKOR 40 mm f/2.8G. Jellyfish were caught from the aquarium approximately 3 h after feeding with artemia when the gastrovascular canals were colored orange from the digested artemia. When they reach about 2.5 cm in diameter, jellyfish were anesthetized with magnesium chloride dissolved in water having the same salinity as the artificial seawater in which they are swimming. To anesthetize the jellyfish, the volume of the jellyfish with seawater was doubled with the magnesium chloride solution. Then, they are placed in a Petri dish in shallow seawater with the sub umbrella facing up. The images are taken by transillumination.

6.3 Histology

The histological section shown in Figure 2B was made for a preparation of observations with transmission electron microscopy. In short, whole juvenile jellyfish are fixed with a 5% glutaraldehyde solution in a 0.1 mol/L cacodylate solution overnight at 4°C [28]. After rinsing with 0.5 mol/L cacodylate solution (overnight at 4°C), the solution is replaced gradually by ethanol 95% after which it is transferred to 95% ethanol containing eosin, in order to stain the jellyfish. Then, the samples are placed in 100% ethanol which is subsequently gradually replaced by a pure molten wax solution. These samples are then cut by a microtome into thin lamellae of about 4 µm thickness. Longitudinal sections of juvenile jellyfish were sliced, starting the sections from the edge of the umbrella, and advancing towards the center of the jellyfish. Figure 2B shows a longitudinal section through a canal and the endoderm of a juvenile jellyfish of approximately 1 cm diameter. The section was visualized under a light microscope (Leica DMI-3000 B), a ×20 magnification objective, and a CCD camera (Andor, iXon3 885).

6.4 Canal diameter deformation measurements

Juvenile jellyfish (n = 7) of about 1 cm in diameter were filmed (30 frames per second) using a Leica inverse microscope (LEICA DMI-3000 B) with a ×20 objective (HCX PL Fluotar L ×20/0.40). The jellyfish were lying flat with the subumbrella facing down. In this position, jellyfish slightly contract occasionally. Two canals were filmed simultaneously. The older and younger canals were identified by looking at the canal network pattern. Off line, diameters were measured before and during contraction at three different positions along the canal and were averaged. Deformation of the canal was calculated by the ratio of the difference in diameter before and during contraction and the diameter before contraction, multiplied by 100. We used one-way repeated measures Anova, followed by a Student–Newman–Keuls test for pairwise multiple comparison to show the statistical difference between the deformation of the older canals versus the younger canals (SigmaPlot 12.5).

6.5 Numerical simulation

Numerical simulations were performed with finite elements toolbox COMSOL Multiphysics 3.5a [29]. We approximated the endoderm and the canals as 2D surface elements with different stiffness.

The simulations were performed on a small piece of a ring at the edge of a circular disk with a radius of 5 mm, with a radial length of 1 mm and with a 12° angle. The geometry of the canals and sprout were chosen to be coherent with our observations in a juvenile jellyfish of 1 cm diameter. The geometry with the simulation mesh is shown in the Supplementary Figure S7A.

We assume the endoderm as a flat rigid incompressible elastic sheet with Young's modulus $E_{en} = 100\,Pa$. The incompressibility of a material corresponds to a Poisson's ratio of 0.5. However, Hooke's law is only valid for Poisson's ratio <0.5. Hence, in our model, we approximate the incompressibility of the endoderm by setting its Poisson's ratio $\nu_{en} = 0.49$. The simulations in 2D imply the absence of out of plane buckling. This assumption is justified for small juveniles at the onset of contraction since the endoderm is held in plane by the mesoglea located above and below.

We modeled the canals in 2D by a slightly compressible elastic membrane, with lower Young's moduli than the endoderm. The young's modulus of the young canal is assumed to be stiffer with $E_{yc} = 30\,Pa$ than the old canal, $E_{oc} = 10\,Pa$. The Poisson's ratio of the canals equals 0.3 ($\nu_{yc} = \nu_{oc} = 0.3$), which allows for compression. It should be noted that the distribution of these stresses does not depend on the values of the Young modulus of the endoderm and the canals but only on the ratio of these values.

We observed that by choosing the elastic modulus of the canals 10 times lower than the endoderm, we obtained rates of reduction of the diameter of the ducts close to those observed *in vivo* (Figure 2B).

To simulate the muscular orthoradial contraction, we impose a reduction of the radial position of the outer circular boundary (at the ring canal). The sides of the ring slice can slip along the radial axis only, and the inner circular boundary is free to move ($\sigma(\epsilon).n = 0$, with n being the outer normal of the boundary).

The simulation was performed quasi-statically, meaning that each simulation step is in a dynamic equilibrium. The relative influence of inertia and elasticity on the system can be determined by computing the Cauchy dimensionless number $C = \frac{\rho V^2}{E}$, with ρ the density of the tissues and V local flow velocity. In our model, $V \approx 200$ µm/s, $\rho = 1{,}000$ kg/m^3 and E ranges from 10 to 100 Pa. Thus, $C<<1$ and the acceleration term $\rho\frac{\partial^2 u}{\partial t^2}$ is always negligible relatively to the elasticity term $div(\sigma(\epsilon))$. As a consequence, we can perform a quasi-static analysis: we solve the static equation $div(\sigma(\epsilon)) = 0$ with a maximal displacement of 200 µm of the outer circular boundary. Then, we reconstruct the time dynamics, thanks to the linearity of the equation relatively to the condition at this boundary.

We selected the mesh size so that a refinement of the mesh did not improve significantly the quality of the results. The mesh consisted in 7,563 triangular elements. The computation time was less than 1 s on an 3.7 GHz 2 Ghz Intel Xeon Gold 6,138.

The different values of the Young's and Poisson's moduli of the different elements under compression results in a distribution of stresses (σ_x, σ_y, σ_{xy}) which are accumulated at the tip of the sprout. The von Mises stresses (σ_{vm}), obtained by combining these different stresses [29], give a satisfactory scalar representation of the stress distribution in the endoderm:

$$\sigma_{vm} = \sqrt{\sigma_x{}^2 - \sigma_x\sigma_y + \sigma_y{}^2 + 3\sigma_{xy}{}^2}.$$

Data availability statement

The original contributions presented in the study are included in the article/Supplementary Material; further inquiries can be directed to the corresponding author.

Author contributions

SS performed the experiments, analyses of the network, in particular for the clones, and wrote the manuscript. SŻ performed the experiments, analyzed the growth dynamics, in particular for the breakthrough event, and wrote the manuscript. CG performed the experiments, in particular for the anatomy, analyses, in particular the contractions, and mechanical modeling and performed mechanical numerical simulations. PD performed mechanical numerical simulations. BM defined the numerical simulations and wrote the manuscript. SD analyzed the patterns and wrote the manuscript. AC directed the work, performed experiments, analyses, and modeling, and wrote the manuscript.

Funding

This work was supported by The LABEX "WHO AM I?" (No. ANR-11-LABX-0071) with a PhD fellowship for SS (doctorants 2015) and a collaborative grant (Projets collaboratifs 2013-II) and by the Mission for Transversal and Interdisciplinary Initiatives (MITI) of the French National Centre of Scientific Research (CNRS), AAP Auto-organisation 2021 and 2022.

Acknowledgments

The authors thank Carine Vias and Léna Zig for their excellent care for the jellyfish. They thank Vincent Fleury for pointing to them this biological system.

Conflict of interest

The authors declare that the research was conducted in the absence of any commercial or financial relationships that could be construed as a potential conflict of interest.

Publisher's note

Supplementary material

The Supplementary Material for this article can be found online at: https://www.frontiersin.org/articles/10.3389/fphy.2022.966327/full#supplementary-material

References

1. Collinet C, Lecuit T. Programmed and self-organized flow of information during morphogenesis. *Nat Rev Mol Cel Biol* (2021) 22(4):245–65. doi:10.1038/s41580-020-00318-6

2. Clément R, Blanc P, Mauroy B, Sapin V, Douady S. Shape self-regulation in early lung morphogenesis. *PLoS ONE* (2012) 7(5):e36925. doi:10.1371/journal.pone.0036925

3. Turing AM. The chemical basis of morphogenesis. *Philos Trans R Soc Lond Ser B, Biol Sci* (1952) 237(641):37–72. doi:10.1098/rstb.1952.0012

4. Southward AJ. Observations on the ciliary currents of the jelly-fish aurelia-aurita L. *J Mar Biol Assoc U K* (1955) 34(2):201–16. doi:10.1017/s0025315400027570

5. Russell FS. *The medusae of the British isles. Vol.Ii - pelagic scyphozoa with a supplement to the firts volume on hydromedusae*. Cambridge: Cambridge University Press (1970).

6. Fuchs B, Wang W, Graspeuntner S, Li Y, Insua S, Herbst E-M, et al. Regulation of polyp-to-jellyfish transition in Aurelia aurita. *Curr Biol* (2014) 24(3):263–73. doi:10.1016/j.cub.2013.12.003

7. Gambini C. *La morphogenaise gastrovasculaire de La méduse Aurelia aurita*. Paris: Université Paris Diderot (2012).

8. Gambini C, Abou B, Ponton A, Cornelissen AJ. Micro- and macrorheology of jellyfish extracellular matrix. *Biophysical J* (2012) 102(1):1–9. doi:10.1016/j.bpj.2011.11.4004

9. Thomé H, Rabaud M, Hakim V, Couder Y. The saffman–taylor instability: From the linear to the circular geometry. *Phys Fluids A: Fluid Dyn* (1989) 1(2):224–40. doi:10.1063/1.857493

10. Clément R, Douady S, Mauroy B. Branching geometry induced by lung self-regulated growth. *Phys Biol* (2012) 9(6):066006. doi:10.1088/1478-3975/9/6/066006

11. Douady S, Lagesse C, Atashinbar M, Bonnin P, Pousse R, Valcke P. A work on reticulated patterns. *Comptes rendus de l'Académie des Sci Série IIb, Mécanique, physique, astronomie* (2020) 348(6-7):659–78. doi:10.5802/crmeca.47

12. Risau W. Mechanisms of angiogenesis. *Nature* (1997) 386(6626):671–4. doi:10.1038/386671a0

13. Katifori E, Szöllősi GJ, Magnasco MO. Damage and fluctuations induce loops in optimal transport networks. *Phys Rev Lett* (2010) 104(4):048704. doi:10.1103/PhysRevLett.104.048704

14. Konkol A, Schwenk J, Katifori E, Shaw JB. Interplay of river and tidal forcings promotes loops in coastal channel networks. *Geophys Res Lett* (2022) 49(10):49. doi:10.1029/2022GL098284

15. Ronellenfitsch H, Katifori E. Phenotypes of vascular flow networks. *Phys Rev Lett* (2019) 123(24):248101. doi:10.1103/PhysRevLett.123.248101

16. Fender ML, Lechenault F, Daniels KE. Universal shapes formed by two interacting cracks. *Phys Rev Lett* (2010) 105(12):125505. doi:10.1103/PhysRevLett.105.125505

17. Couder Y, Pauchard L, Allain C, Adda-Bedia M, Douady S. The leaf venation as formed in a tensorial field. *Eur Phys J B* (2002) 28(2):135–8. doi:10.1140/epjb/e2002-00211-1

18. Bohn S, Pauchard L, Couder Y. Hierarchical crack pattern as formed by successive domain divisions. *Phys Rev E* (2005) 71(4):046214. doi:10.1103/PhysRevE.71.046214

19. Milinkovitch MC, Manukyan L, Debry A, Di-Poï N, Martin S, Singh D, et al. Crocodile head scales are not developmental units but emerge from physical cracking. *Science* (2013) 339(6115):78–81. doi:10.1126/science.1226265

20. Li B, Li F, Puskar KM, Wang JH. Spatial patterning of cell proliferation and differentiation depends on mechanical stress magnitude. *J Biomech* (2009) 42(11):1622–7. Epub 20090530. doi:10.1016/j.jbiomech.2009.04.033

21. Shraiman BI. Mechanical feedback as a possible regulator of tissue growth. *Proc Natl Acad Sci U S A* (2005) 102(9):3318–23. doi:10.1073/pnas.0404782102

22. Budek A, Kwiatkowski K, Szymczak P. Effect of mobility ratio on interaction between the fingers in unstable growth processes. *Phys Rev E* (2017) 96(4):042218. doi:10.1103/PhysRevE.96.042218

23. Al-Kilani A, Lorthois S, Nguyen TH, Le NF, Cornelissen A, Unbekandt M, et al. During vertebrate development, arteries exert a morphological control over the venous pattern through physical factors. *Phys Rev E* (2008) 77(5):051912. doi:10.1103/PhysRevE.77.051912

24. le Noble F, Fleury V, Pries A, Corvol P, Eichmann A, Reneman RS. Control of arterial branching morphogenesis in embryogenesis: Go with the flow. *Cardiovasc Res* (2005) 65(3):619–28. doi:10.1016/j.cardiores.2004.09.018

25. Nguyen TH, Eichmann A, Le NF, Fleury V. Dynamics of vascular branching morphogenesis: The effect of blood and tissue flow. *Phys Rev E* (2006) 73(6):061907. doi:10.1103/PhysRevE.73.061907

26. Khalturin K, Shinzato C, Khalturina M, Hamada M, Fujie M, Koyanagi R, et al. Medusozoan genomes inform the evolution of the jellyfish body plan. *Nat Ecol Evol* (2019) 3(5):811–22. doi:10.1038/s41559-019-0853-y

27. Kroiher M, Siefker B, Berking S. Induction of segmentation in polyps of Aurelia aurita (scyphozoa, Cnidaria) into medusae and formation of mirror-image medusa anlagen. *Int J Dev Biol* (2003) 44(5):485–90. doi:10.2108/zs160161

28. Chapman DM. Microanatomy of the bell rim of Aurelia aurita (Cnidaria: Scyphozoa). *Can J Zool* (1999) 77:34–46. doi:10.1139/z98-193

29. COMSOL. *Comsol Multiphysics®*. 3.5a ed. Stockholm, Sweden: Comsol A.B (2019).